water

MDPI

Article

Hydrogeological Investigation of a Goaf and Subsidence Area Based on a Ground-to-Air Transient Electromagnetic Sounding Method

Qicai Feng [1], Chang Li [2,*], Shuren Hao [3,4], Dongsheng Li [5], Tao Liu [2], Zhonglin Sun [2] and Ling Zhou [6]

[1] Sixth Geological Exploration Institute of Heilongjiang Province, Jiamusi 154002, China; ffqqcc510@163.com
[2] Harbin Center for General Survey of Natural Resources, CGS, Harbin 150081, China; huangjinliutao@163.com (T.L.); sunzhonglin@mail.cgs.gov.cn (Z.S.)
[3] School of Civil and Architectural Engineering, East China University of Technology, Nanchang 330013, China; dr_haosr@163.com
[4] Engineering Research Center for Geological Environment and Underground Space of Jiangxi Province, East China University of Technology, Nanchang 330013, China
[5] College of Instrumentation & Electrical Engineering, Jilin University, Changchun 130000, China; 17790096370@163.com
[6] School of Civil Engineering, Shandong Jianzhu University, Jinan 250101, China; zhongling20@sdjzu.sdu.cn
* Correspondence: lichang@mail.cgs.gov.cn

Abstract: Water hazards in coal mines have always been the main geological hazard that restricts the safety of coal mine production. The traditional electromagnetic method is difficult to accurately detect the hydrogeological conditions of underground goafs due to accuracy and interference problems. The ground-to-air transient electromagnetic method is an electromagnetic detection technology with strong adaptability to various terrains, a large detection depth, a wide coverage, a high resolution, and fast speed. This paper mainly applies the ground-to-air transient electromagnetic method to conduct a hydrogeological engineering geological survey in a mine subsidence area. By using this method effectively, changes in hydrogeological and engineering geological conditions in the mine subsidence area are identified and water filling conditions below section 310 and section 250 of the roadway are determined. This study provides accurate and reliable basic data support for rescue operations and post-disaster reconstruction efforts, while also offering valuable insights for similar exploration projects.

Keywords: ground-to-air transient; electromagnetic detection; subsidence area; hydrogeological condition

Citation: Feng, Q.; Li, C.; Hao, S.; Li, D.; Liu, T.; Sun, Z.; Zhou, L. Hydrogeological Investigation of a Goaf and Subsidence Area Based on a Ground-to-Air Transient Electromagnetic Sounding Method. *Water* **2024**, *16*, 1067. https://doi.org/10.3390/w16071067

Academic Editor: Juan José Durán

Received: 18 February 2024
Revised: 1 April 2024
Accepted: 2 April 2024
Published: 7 April 2024

1. Introduction

The transient electromagnetic method (TEM) is a method to investigate underground resources by creating an artificial electromagnetic field source in the time domain [1–5]. It is suitable for underground mineral resource exploration, hydrogeological exploration, engineering geological exploration, and groundwater resource exploration. It has also been widely used in the detection of swamp areas, desert areas, karst areas, goafs, subsidence areas, and other areas [6–10]. The transient electromagnetic method is divided into the transient ground electromagnetic method, the transient airborne electromagnetic method, and the transient ground-to-air electromagnetic method [11–14]. The transient electromagnetic ground method has the advantages of a large detection depth and a high resolution [15–17]. The transient airborne electromagnetic method has the advantages of strong terrain adaptability, a wide detection range, and fast speed [18,19]. The ground-to-air transient electromagnetic method integrates ground and aerial detection, combining

the advantages of both the transient ground-to-air electromagnetic method and the transient airborne electromagnetic method. It exhibits exceptional adaptability to various terrains, offers a substantial detection depth, covers a wide range, provides high resolution, and operates at a fast speed.

The working mode of the ground-to-air transient electromagnetic method was initially proposed by Nabighian in 1988, focusing on the utilization of a horizontal electric dipole source [20], which aimed to investigate geological conditions beneath conductive surface cover in arid regions of Australia and also aimed to effectively address challenges associated with deep exploration. Elliot further advanced this technique by developing a fixed loop airborne transient electromagnetics system (FLAIRTEM) [21,22]. In order to address the challenge of conducting deep exploration in areas characterized by significant surface fluctuations, Mogi et al. are actively seeking out deep-seated metal deposits and geothermal resources. Consequently, they have developed a grounded electrical source airborne transient electromagnetics (GREATEM) system [23]. A team from Jilin University has developed a time domain ground-to-air electromagnetic exploration system utilizing a long wire source for an unmanned airship. This system bears resemblance to the GREATEM system; however, it distinguishes itself by employing an unmanned airship as a carrier to transport an electromagnetic receiving system and capture the transient response of the magnetic field's time derivative [24]. The wavelet denoising method for the system was investigated by Li Suyi et al. (2013). By employing the sym8 wavelet base based on the principle of wavelet multi-resolution analysis, noise suppression was effectively achieved and the quality of resistivity imaging in electromagnetic data was enhanced [25]. Ji Yanju et al. (2013) conducted a water resource detection experiment in the Bayan Baolig area of Inner Mongolia and compared the treatment results with those obtained from ground transient electromagnetic and magnetotelluric methods. The findings demonstrated that the system accurately depicted the subsurface electrical structure and effectively differentiated geological anomalies, thus confirming the method's efficacy [26].

The occurrence of water disasters in coal mines has persistently posed significant geological hazards that hinder secure coal production, with its influence being surpassed solely by coal and gas outbursts [27]. Amongst diverse manifestations of water damage, goaf water indisputably occupies a pre-eminent position due to its frequent incidence, resulting in substantial human casualties and property losses [28,29]. Especially during the rainy season, there is a temporal escalation of moisture within the goaf region, which intensifies the peril associated with the potential harm caused by excessive groundwater infiltration. Consequently, meticulous attention should be devoted to investigating goaf waters, as they play an indispensable role in ensuring that subsequent mining operations remain safe.

This paper presents a ground-to-air time domain electromagnetic detection system, consisting of the following two components: a ground launching system and an airborne receiving system. The system demonstrates characteristics such as a sensitive response to conductive electrolytes, a high detection efficiency, minimal blind spots in detection, a strong anti-interference capability, a significant detection depth, a non-contact detection ability, cost-effectiveness, and adherence to high safety standards. Non-contact detection effectively addresses the challenges faced by conventional geophysical exploration in complex terrains and geomorphological conditions. The system was utilized for detecting and analyzing subsidence areas caused by mining activities. It accurately measured and delineated the extent and nature of the subsidence area resulting from accidents, while identifying changes in hydrogeological and engineering geological conditions within the affected mine subsidence area. Furthermore, the water filling situation below sections 310 and 250 of the roadway middle section was successfully determined, thus providing precise and reliable foundational data support for rescue operations, as well as post-disaster reconstruction efforts. Additionally, this study offers valuable insights that can be applied to similar exploration projects.

2. Ground-to-Air Transient Electromagnetic Detection Principle

2.1. Instruments and Equipment

The JL-GAEM multifunctional ground-to-air electromagnetic exploration system, independently developed by Jilin University, was selected as the transient electromagnetic exploration instrument for ground-to-air applications. Comprising a ground launching system and an airborne receiving system, the JL-GAEM ground-to -air electrical sounding system is highly versatile.

The ground launch system achieves joint time–frequency domain measurements through coded transmission. The system is capable of achieving two assembly modes, as follows: on-board integration and split assembly. On-board integration refers to the customization of the body, while internal integration encompasses all modules such as generators. Each module of the split launch system can be divided into independent units, allowing for enhanced flexibility in transportation and assembly methods. Additionally, the equipment is capable of reaching inaccessible test areas, which conventional vehicles cannot access. Figure 1 illustrates a 200 KW high-power power vehicle integrated with a launch system.

Figure 1. Vehicle-mounted integrated transmitter.

The integrated receiving system for airborne transient electromagnetic detection consists of the following three components: a single/three-component hollow coil induction sensor, a multi-channel receiver, and a ground detection station. The system is triggered synchronously based on GPS and allows for remote control over the switch between the time domain and frequency domain. It possesses characteristics such as low noise, low power consumption, and high precision. Figure 2 illustrates a ground-to-air single-component transient electromagnetic detection and receiving system based on a rotary-wing UAV.

Figure 2. Ground-to-air electromagnetic signal receiving system based on rotary-wing UAV.

2.2. Detection Principle

The ground-to-air transient electromagnetic detection method is an additional novel method of electromagnetic detection, following the ground-to-air and airborne electromagnetic methods. The proposed method employs a high-power artificial electromagnetic source, positioned on the ground, as an exciting field generator, while capturing magnetic field signals in the air to facilitate efficient exploration of the geoelectrical structure [30,31]. The proposed method exhibits high efficiency and low cost, while also considering the detection accuracy of ground-based methods. Moreover, it is not constrained by terrain or landform, enabling the non-contact rapid detection of complex surface conditions. The working principle of the ground-to-air time–frequency electromagnetic detection method is illustrated in Figure 3.

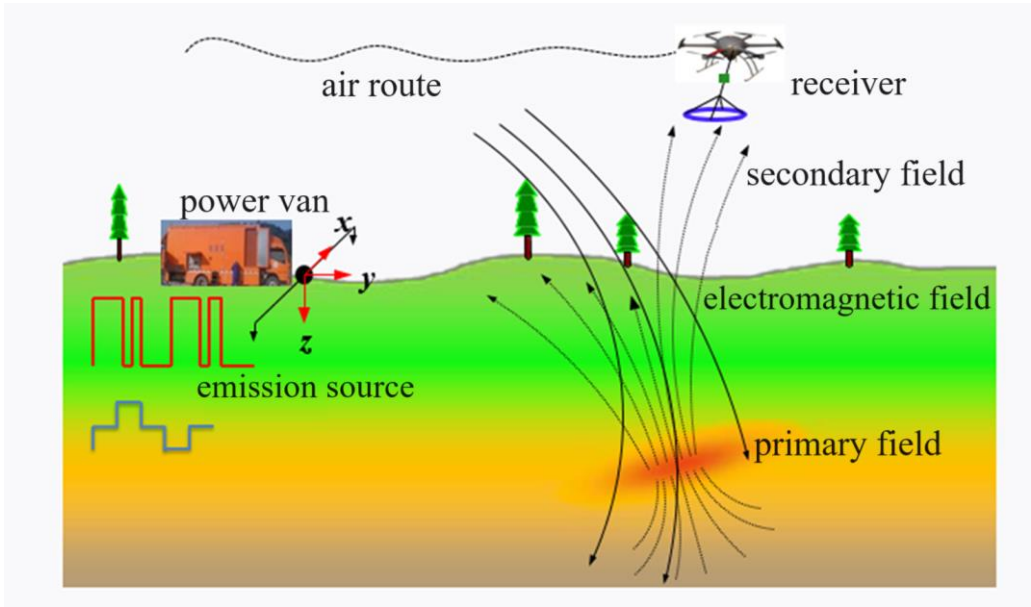

Figure 3. Working principle of ground-to-air transient electromagnetic method.

The ground-to-air transient electromagnetic detection technique not only offers significant advantages in terms of increased depth and enhanced resolution, but also provides a wide range and rapid speed for airborne transient electromagnetic detection. The

technology is particularly well-suited for resource exploration in challenging terrains such as mountainous areas, forested areas, swamps, and other unique landscapes in China [32–34]. The ground-to-air transient electromagnetic detection system utilizes a long grounded wire, positioned on the ground, as the emission source, generating a primary field through current flow. Subsequently, the receiving sensor mounted on the aircraft captures and analyzes the induced vertical electromagnetic field resulting from turning off this current, thereby extracting information pertaining to underground electrical structures. The method is well-suited for exploring low-resistivity anomalies (20~800 m) in shallow and intermediate layers. It is characterized by its high construction efficiency and robust anti-interference capability.

The ground-to-air transient electromagnetic probe enables the acquisition of the apparent resistivity curve within a specified time window, with the primary focus being on the temporal rate of change of the magnetic field, commonly referred to as dB/dt. The initial apparent resistivity corresponds to the shallow subsurface information, while the final apparent resistivity corresponds to the deeper subsurface information. Due to its relatively high construction efficiency, this method enables the three-dimensional exploration of a given work area. The transient electromagnetic detection method is extensively employed in various industries such as mining and coal mining. Typically, the observation area for ground-to-air transient electromagnetic exploration is within the mid-to-near range, as illustrated in Figure 4, depicting the relationship between reception and emission.

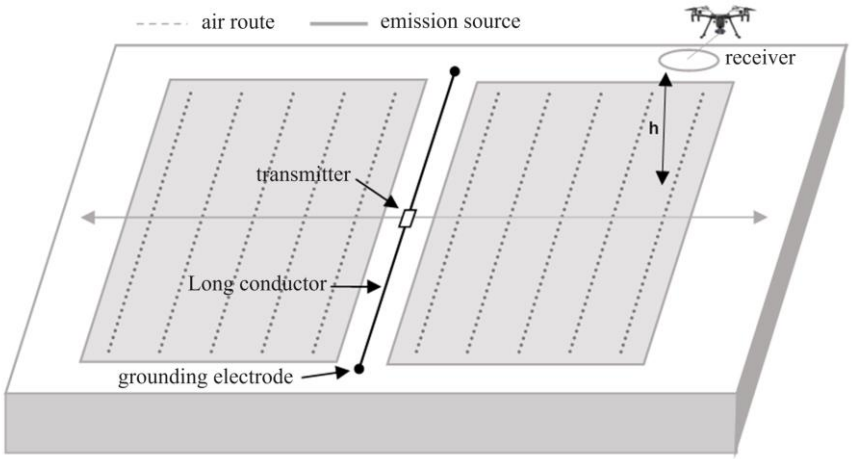

Figure 4. Schematic diagram of ground-to-air transient electromagnetic method.

As is shown in Figure 5, the primary procedure for data processing and interpretation of the ground-to-air transient electromagnetic method is as follows:

1. Data preprocessing: including data interception, evaluation, and superposition; noise treatment and baseline correction; and time domain signal data pumping.
2. Obtaining the ground electrical parameters: based on the obtained comprehensive superposition signal, convert it into a time-varying apparent resistivity curve.
3. Apparent resistivity-depth imaging involves filtering the apparent resistivity curve, suppressing interference, and applying other processing techniques to obtain reliable apparent resistivity-depth data. By analyzing the relative changes in electrical properties within the measurement area based on known logging and seismic data, a preliminary understanding of the geological structure of the section is achieved, resulting in the generation of resistivity-depth profiles and slice maps.

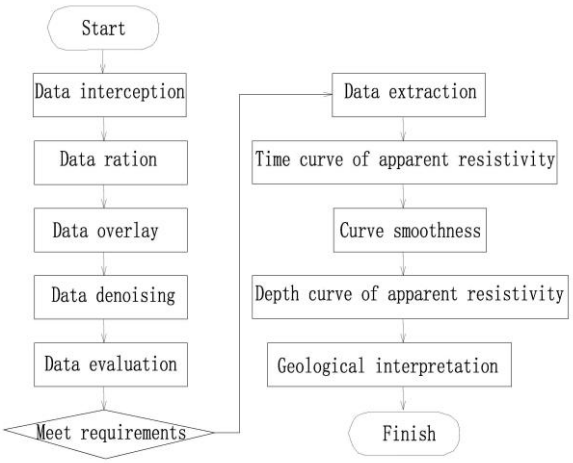

Figure 5. Data processing flowchart of ground-to-air transient electromagnetic method.

2.3. Calculation Principles

In order to represent the resistivity distribution of underground media in the form of an apparent solar rate–apparent depth map, it is necessary to calculate the apparent solar rate–apparent depth through electromagnetic data. KAUFAMN (1983) and WEIR (1980) gave the z-direction magnetic field response of an electric dipole source in a uniform half-space [35,36].

$$\frac{\partial H_z}{\partial_t} = \frac{Ids}{8\pi t\theta^2}\frac{y}{r^5}\left[3erf\left(\theta r\right) - \frac{2}{\pi^{1/2}}\theta r\left(3+2\theta^2 r^2\right)e^{-\theta^2 r^2}\right] \tag{1}$$

where H is the vertical magnetic field intensity; y is the vertical coordinate; I is the current intensity; ds is the length of the electric dipole; t is the sampling time; r is the distance from the receiver to the electric dipole; θ is a function of the electrical conductivity ρ; and erf is the error function.

$$\theta = \sqrt{\frac{\mu\sigma}{4t}} \tag{2}$$

Equation (1) is utilized by substituting the receiving coil area S and $Bz = \mu H_z$ (where Bz represents the magnetic induction intensity and μ denotes the permeability). By superimposing the response of multiple electric dipoles, the expression for electromagnetic response in the Z direction of the grounded long wire is obtained as shown in Equation (3). Solving Equations (2) and (3) enables the determination of conductivity σ.

$$V_z\sum_{i=1}^{N}\frac{ISds\mu}{8\pi t\theta^2}\frac{y}{r_i^5}\left[3erf\left(\theta r_i\right) - \frac{2}{\pi^{1/2}}\theta r_i(3+2\theta^2 r_i^2)e^{-\theta^2 r_i^2}\right],$$
$$r_i = \sqrt{(x - x_i)^2 + y^2} \tag{3}$$

where r_i is the distance between the receiver and the i-th electric dipole, and x_i is the distance between the i-th electric dipole and the midpoint of the long conductor source.

3. Overview of the Study Area and Detection Results

3.1. Overview of the Study Area

3.1.1. Geological Conditions of the Study Area

The study area is characterized by the presence of the Wu5-Guansongzhen middle uplift belt (subclass I, IV 2) within the northern part of the Yichun–Yanshou geosyncline fold system (IV), as shown in Figure 6. In close proximity to the mining area, there have been multiple stages of granitoid intrusion, particularly during the middle Caledonian and early Yanshan periods. These intrusions have resulted in the formation of trap bodies within Paleozoic strata and the Lower Cambrian Yanshan Formation that are associated with mineralization. However, it should be noted that the exposed area is relatively limited.

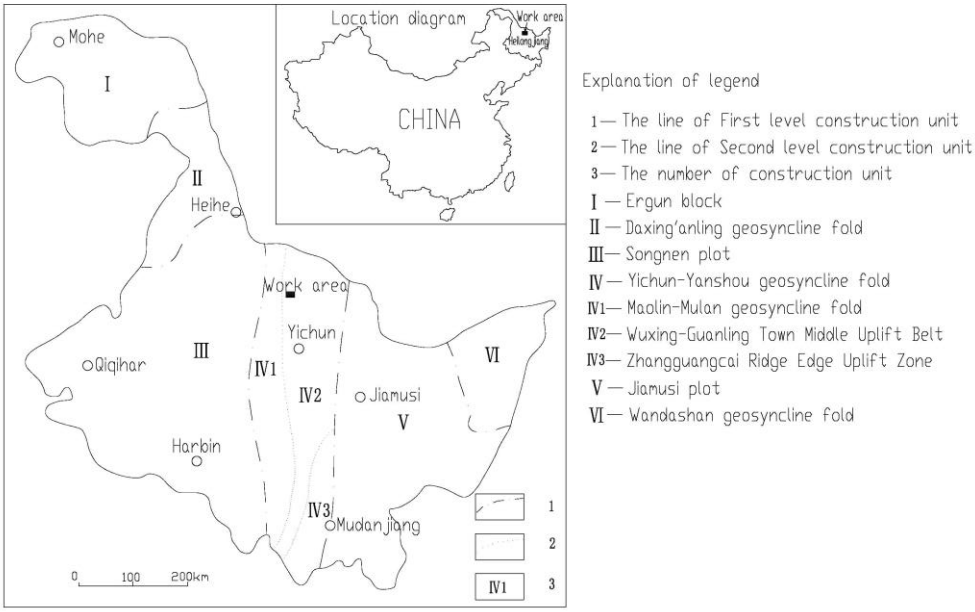

Figure 6. Schematic map of tectonic zones in Heilongjiang Province.(from Exploration report of No. I magnetic-rich ore body of Cuihongshan iron polymetallic deposit, Xunke County, Heilongjiang Province).

In the study area, the outcrop layer is small and simple, consisting of only the Lower Cambrian Yanshan Formation (∈1q) and the fourth system (Q4) loose sand gravel layer. The intrusive rocks are mainly mid-Caledonian (Middle Ordovician) cataclastic granite, mid-Yanshanian (Middle Jurassic) granites, and dike rocks.

The study area is a segment of the NE-Hongchuan complex anticline, measuring 5 km in width; however, the fold morphology has been significantly compromised due to extensive intrusion of granite and prolonged weathering and denudation. The study area is situated within the near NNW tectonic belt, characterized by two groups of conjugate faults oriented in the NE and NW directions. The geological profile is shown in Figure 7. It represents the intrusive contact zone between cataclastic granite and the lower Cambrian Yanshan Formation, exerting control over the spatial distribution of the ore body. The strata exhibit a monoclinal structure, striking at an azimuth of 330° with a dip angle ranging from 60° to 80°. There is slight variation in the trend, and the structural morphology displays a monoclinal pattern with significant variability in orientation.

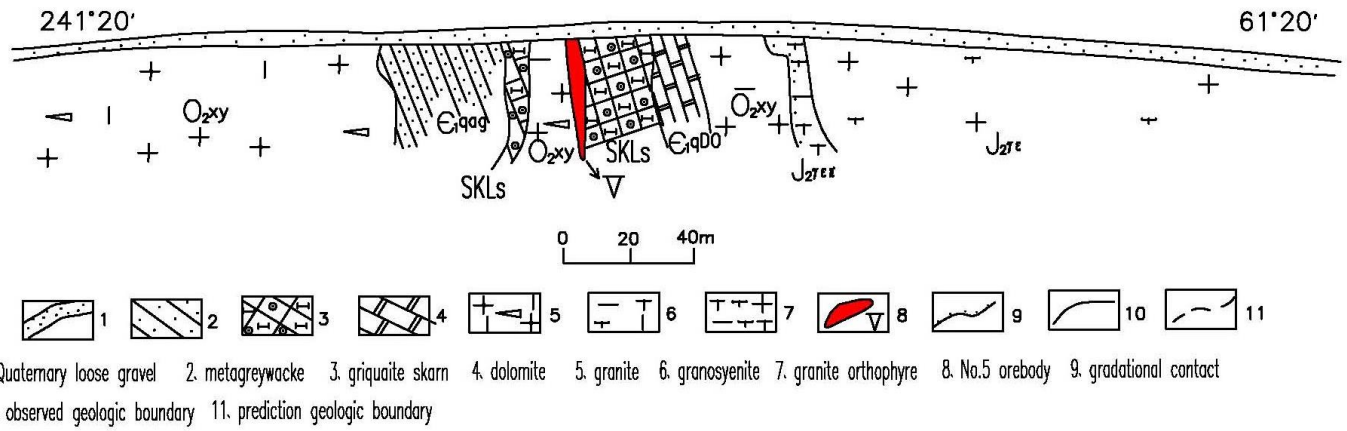

Figure 7. Geological profile of the study area. (from Exploration report of No. I magnetic-rich ore body of Cuihongshan iron polymetallic deposit, Xunke County, Heilongjiang Province)

3.1.2. Hydrogeological Conditions of the Study Area

There are five primary groundwater types identified in the study area, namely pore water of the quaternary alluvial sand and gravel in the valley, shallow network weathered fissure water, non-carbonate dive-like structural fissure water, carbonate dive-like dissolution fissure water, and falling body fissure water formed by caving in goafs (Table 1).

Table 1. Groundwater types in the study area.

Groundwater Type	Aquifer Lithology	Abundant in Water	Trait
Quaternary alluvial sand gravel pore water	Mainly sand, gravel sand, gravel	Strong rich water, the water inflow of a single well is generally 3000~5000 m^3/d.	The aquifer is 400–460 m wide and 35 m thick. The maximum water inflow of a single well is 6907.68 m^3/d. Strong rich water. The hydrochemical type is heavy carbonate-calcium type.
Network weathering crevice water	Crystalline limestone, crystalline dolomite, dolomitic crystalline limestone, granite, skarn, metamorphic sandstone	Weak rich water, single well water inflow is generally 30~300 m^3/d	The thickness of the aquifer is 37.05–73.74 m and the water output from a single hole is 17.19–65.23 m^3/d, with weak water richness. The hydrochemical types are bicabonate-calcium and sodium.
Solution fissure water resembling a carbonate dike	Crystalline limestone, crystalline dolomite, dolomitic crystalline limestone, granite, skarn, metamorphic sandstone	The upper part is moderately rich in water, and the water inflow of a single well is generally 800~1500 m^3/d. The lower part is weak and rich in water, and the water inflow of a single well is generally 10~300 m^3/d	The rich water above 190 m elevation is medium, and the rich water at a deep depth is weak. The hydrochemical types are bicabonate-calcium and sodium.
Fractured water in non-carbonate dike structures	Granite, skarn, metamorphic sandstone	Weak rich water, single well water inflow 10~100 m^3/d	The thickness of the aquifer is 42.98–70.10 m and the water output from a single hole is 7.09–42.16 m^3/d, with weak water richness. The hydrochemical type is heavy carbonate—calcium—sodium type.

Falling body cracking crack water	Dolomitic crystalline limestone	It has strong water richness and water permeability	The thickness of the aquifer is 42.98–70.10 m and the water output from a single hole is 7.09–42.16 m^3/d, with weak water richness. The hydrochemical type is heavy carbonate—calcium—sodium type.

3.1.3. Survey Overview of the Study Area

The water burst occurred in the old goaf on the northwest side of the 310 m middle section of the mine. Within a span of 22 h, both water and mud bursts reached a volume of 300,000 m^3, resulting in the flooding of certain sections of the mine roadway. The collapse pit on the surface measures approximately 80 m in radius and 20 m in depth. Due to its water-filled state, the exact extent of subsidence area and the filling and silting conditions of the underground mining roadway remain unknown, but will be determined through geophysical exploration.

Geophysical technicians have adopted high-density electrical methods, controlled source audio magnetotelluric sounding, and high-precision magnetic methods for exploration. Due to the limited construction conditions, the above geophysical exploration work cannot be carried out on the surface of the collapse pit, and the above geophysical exploration work outside the pit cannot determine the water filling and siltation of the collapse pit and its underground mining roadway, with no obvious detection effect being achieved. The transient electromagnetic method is employed to effectively identify the scope of subsidence area, to determine the location of water permeation, and to assess the condition of water filling and blockage in roadways, as well as to monitor changes in hydrogeological conditions.

3.2. Working Methods and Parameters

3.2.1. Testing Task

The preliminary experiment is designed to determine the final parameters of the exploration system, in accordance with the objectives and requirements of the exploration and by incorporating the principles of the ground-to-air transient electromagnetic method detection. The parameters, including offset, launch current, flight speed, and height of the UAV, were determined through field emission current impact testing, UAV flight speed impact testing, and UAV flight height impact testing on electromagnetic response.

As shown in Figure 8, there is no distortion in the electromagnetic data morphology when the offset distance is 800 m; therefore, it is preferable to choose an offset distance not exceeding 800 m. As shown in Figure 9, the calculated resistivity results are reliable when the offset distance exceeds 150 m. Therefore, the minimum offset distance for this survey is determined to be 150 m. The influence of speed on the amplitude of electromagnetic response is found to be negligible, as demonstrated in Figure 10. Considering the length of the design measurement line and the endurance capabilities of the UAV, a speed of 5 m/s has, ultimately, been selected. As can be seen from Figure 11, the flight altitude has very little influence on the electromagnetic response amplitude. The site altitude of 30 m can meet the flight safety, and the flight altitude of this experiment is determined to be 30 m.

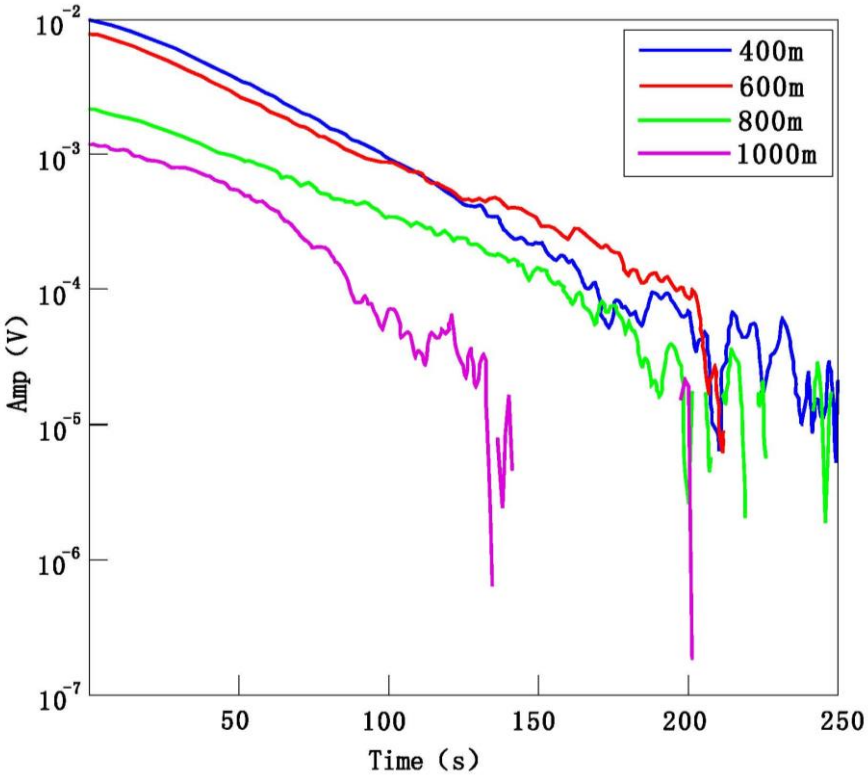

Figure 8. Electromagnetic response of a 30 A emission current at various distances.

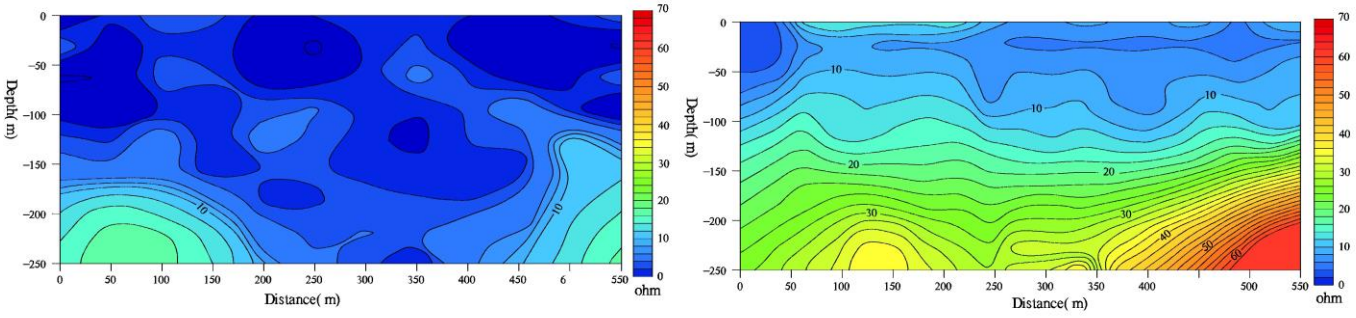

(**a**) (**b**)

Figure 9. Showcases the resistivity imaging outcomes of an identical profile at various observation positions. (**a**) The electrical resistivity imaging results were obtained from a 50 m survey. (**b**) The electrical resistivity imaging results were obtained from a 170 m survey.

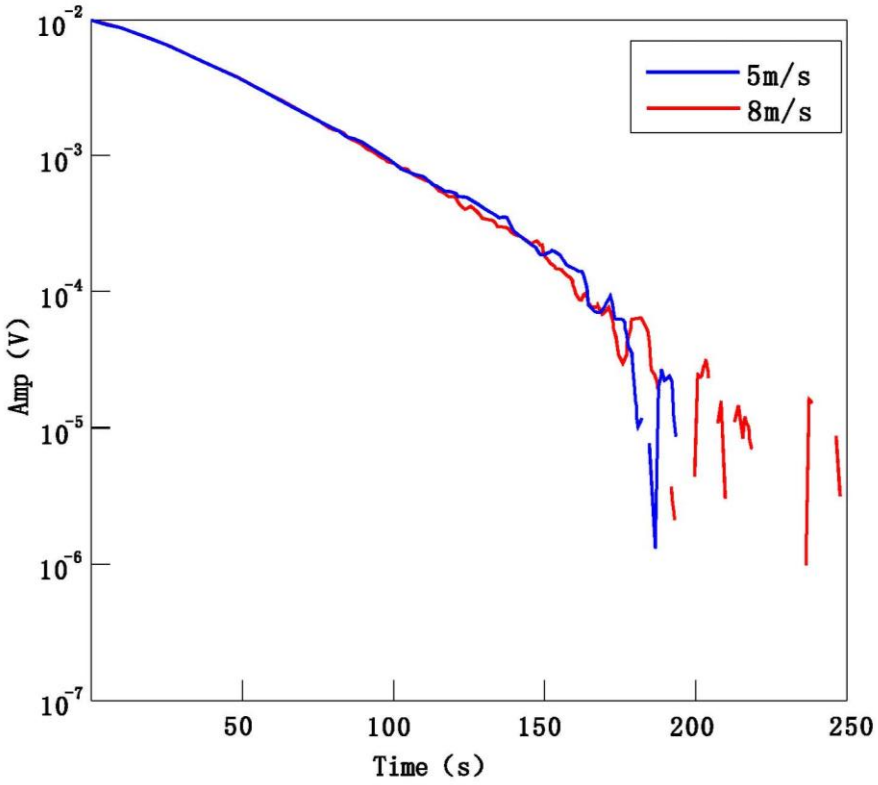

Figure 10. Ground-to-air electromagnetic response of unmanned aerial vehicles at various velocities.

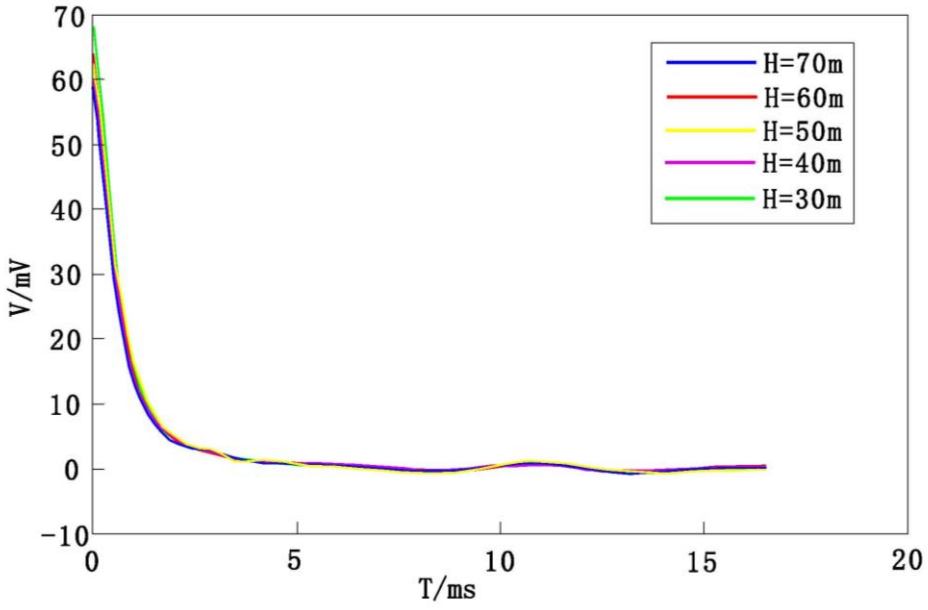

Figure 11. Ground-to-air electromagnetic response of unmanned aerial vehicles at various flight altitudes.

3.2.2. Operating Parameters

Experiments were carried out with parameters such as side distance measurement, emission current, flight speed, flight height, etc. Through comparative analysis, the following specific working parameters used in this experiment were obtained: the distance between the emitter of the electrical source AB = 500 m, AB parallel to the direction of the

measuring line of the working area, the farthest distance between the emitter and the measuring line of the working area is 450 m, the nearest distance is 100 m, the power supply current I = 30 A, the power supply cycle is 8 S, and the actual power supply power is 27 kw. The UAV is set to fly at a height of 30 m and a speed of 5 m/S.

The drones were partially operated manually for takeoff and landing, resulting in a total of 14 flights. Once manually controlled to reach the designated altitude and enter the working area, the drones autonomously followed a predetermined flight path at a consistent speed, while continuously collecting electromagnetic field data. Multiple data points were iteratively acquired before and after each observation point to obtain the final observed data for that specific location. Both the transmitter and receiver coils are equipped with GPS for synchronization.

3.2.3. Engineering Layout

The survey was conducted using a grid spacing of 20 × 20 m, indicating that the measurement lines and points were positioned at intervals of 20 m. The orientation of the measurement lines coincided with that of the exploration lines. Specifically, measurement line 1 corresponded to exploration line 60, while a total of 14 exploration lines were positioned within the range of exploration lines 48 and 60, as illustrated in Figure 12. In total, there were precisely 294 measurement points.

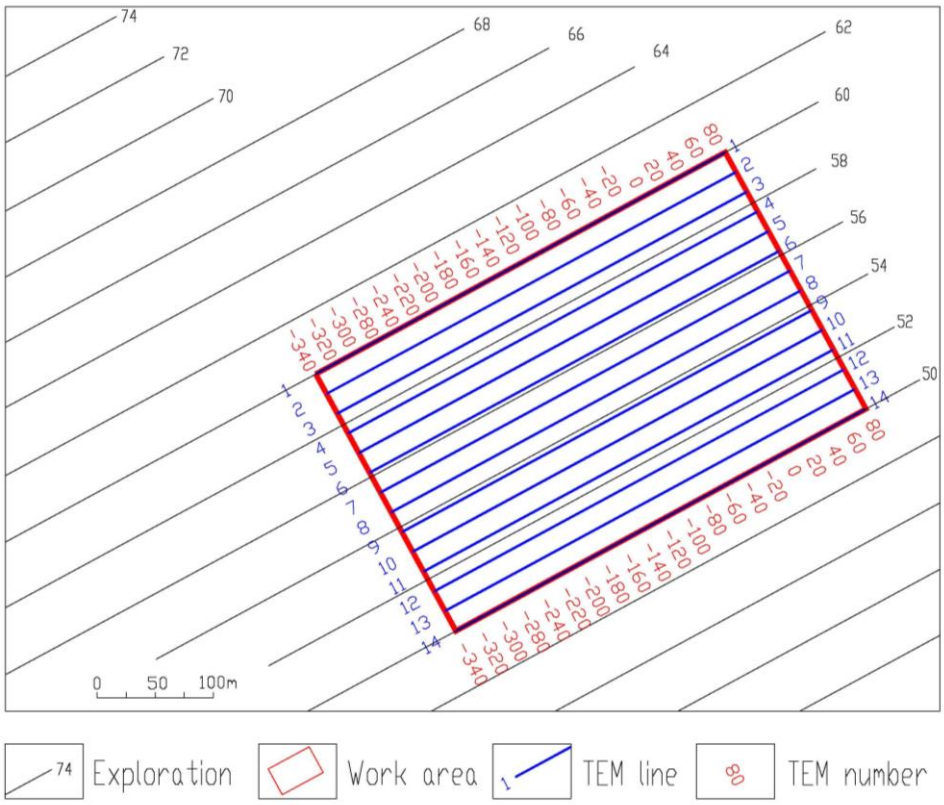

Figure 12. The engineering layout diagram.

3.3. Interpretation of Typical Profiles of Detection Achievements

(1) The Analysis of Profile Results for Test Line 1

After inversion, the profiles of survey lines 1 to 4 exhibit similarities, with variations observed only in subsidence areas and water-filled roadway regions. The interpreted profiles remain fundamentally consistent. The resistivity ranges from 10 to 70 Ω·m and gradually increases with depth. Based on the resistivity variations, a distinct low-resistivity anomaly is observed between −160 m and −70 m, taking the shape of an inverted triangle,

with resistivity values ranging from 10 to 15 Ω·m. It can be inferred that this anomaly represents a subsidence area near the surface, characterized by a collapse depth of approximately 80 m. The apex of the inverted triangle is likely to indicate the point of water permeation. Below this water permeation point (at depths ranging from 80 to 120 m), there exists a horizontal low-resistance anomaly with resistivity variations in the range of 10–20 Ω·m. The low-resistance anomaly corresponds to the 310 middle section tunnel, indicating that it is caused by water infiltration in the 310 middle section tunnel. Refer to Figure 13 for further details.

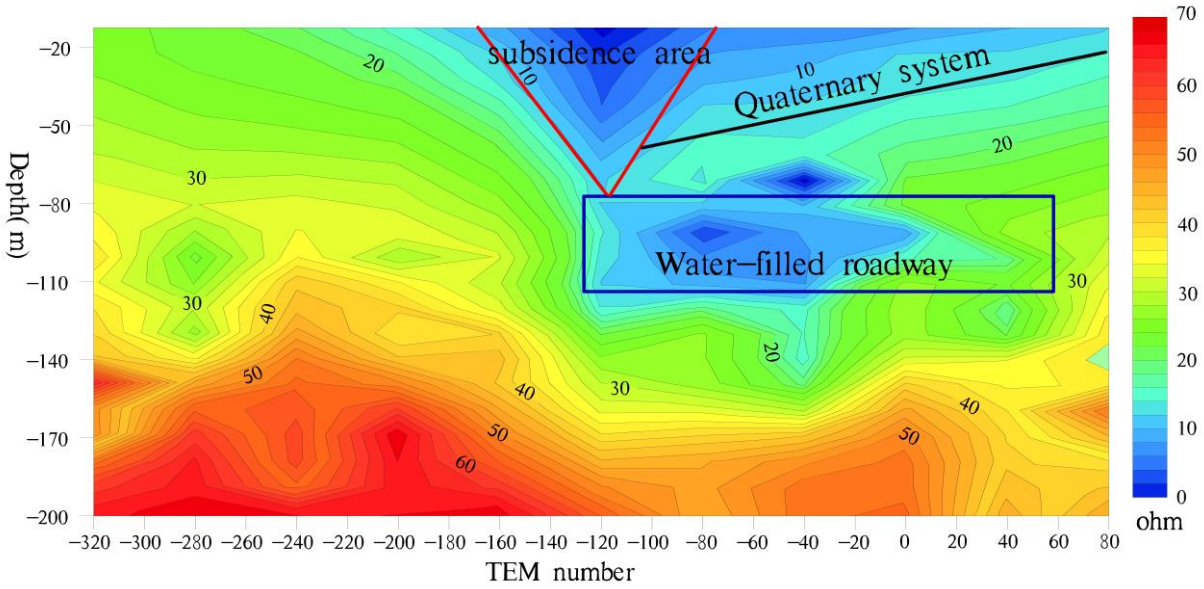

Figure 13. The diagram presents the inversion and interpretation of resistivity in survey line 1.

(2) The Analysis of Profile Results for Test Line 5

The resistivity characteristics of Section 5 of the survey line indicate a significantly increased collapse depth in the subsidence area, measuring approximately 140 m. The subsidence area cannot be distinguished from the mining roadway and is characterized by severe seepage influence. A high-resistivity anomaly zone with horizontal bead-like features is observed at a depth of 140–180 m below the profile surface, which is inferred to represent an unfilled roadway in the middle section 250, not affected by collapse. Refer to Figure 14 for further details.

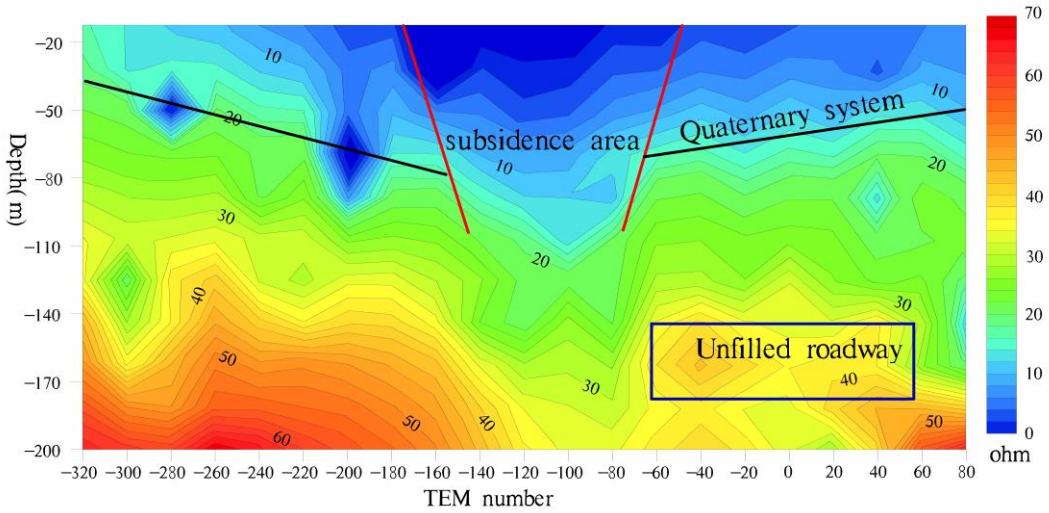

Figure 14. The diagram presents the inversion and interpretation of resistivity in survey line 5.

(3) The Analysis of Profile Results for Test Line 6

The resistivity characteristics of line 6's profile indicate an expansion in the extent of the subsidence area, ranging from −220 to −30 m. The surface width measures approximately 190 m, while the depth of subsidence is estimated at around 120 m. Based on the profile, it can be inferred that the subsidence area is connected to a mining roadway. Specifically, there appears to be a partially filled water-filled section in the middle section of 310 roadway, indicating significant water permeability issues within this affected region, as depicted in Figure 15.

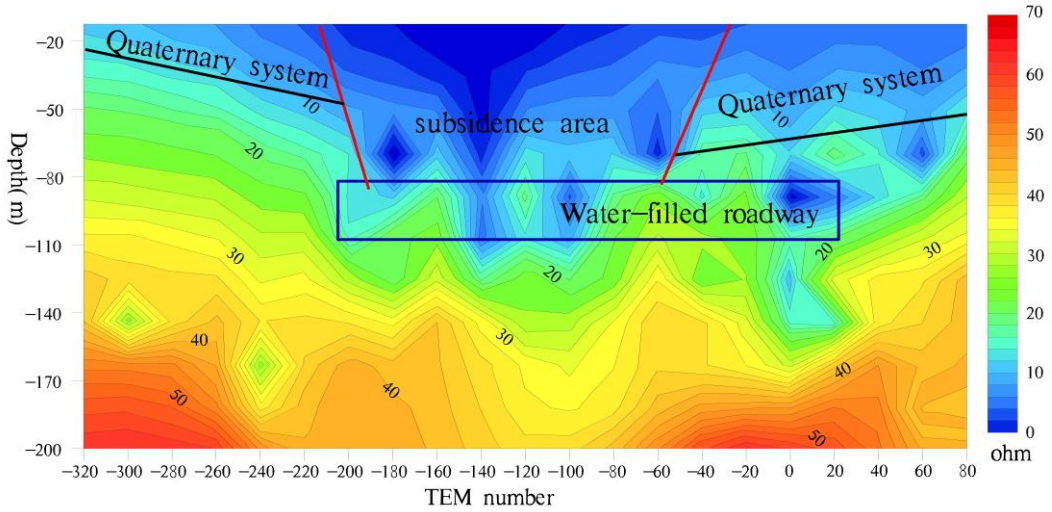

Figure 15. The diagram presents the inversion and interpretation of resistivity in survey line 6.

(4) The Analysis of Profile Results for Test Line 10

The resistivity characteristics of survey line 10 indicate that the subsidence area exhibits no discernible response. Specifically, there is a weakening trend from line 6 to line 10, with the surface low-resistivity layer gradually transitioning into an approximately horizontal distribution. This suggests that the low-resistivity layer primarily represents quaternary features. Two distinct horizontal beaded low-resistivity anomaly zones are identified beneath this layer, corresponding to the mining roadway in the section in the middle of 310 and the section in the middle of 250, respectively. The section in the middle of 310 is affected by subsidence and is partially filled with water, while the middle part of section 250 remains unaffected by subsidence and exhibits a significantly higher resistivity without any noticeable signs of water filling characteristics. For more details, please refer to Figure 16.

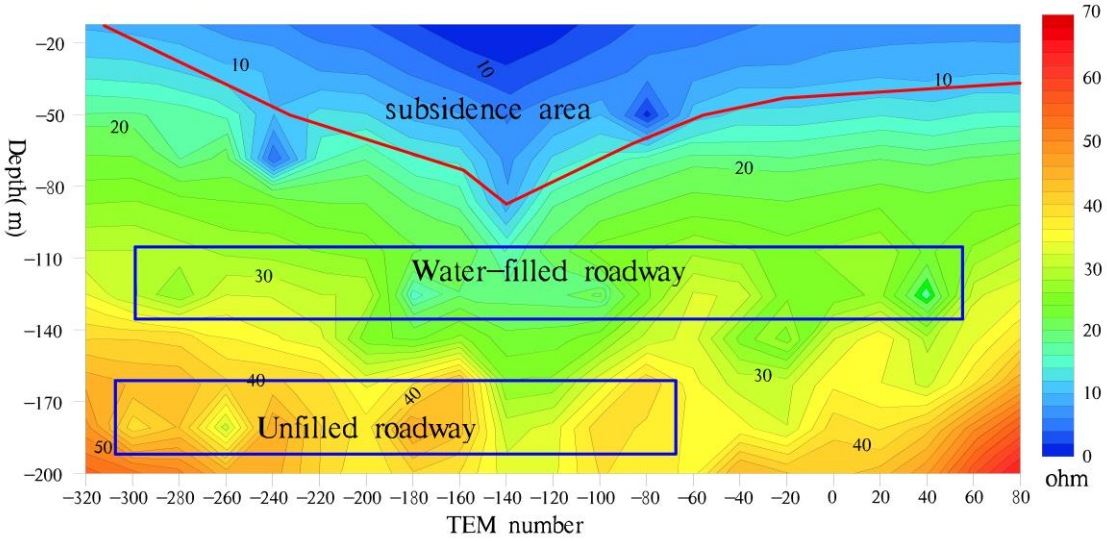

Figure 16. The diagram presents the inversion and interpretation of resistivity in survey line 10.

(5) The Analysis of Profile Results for Test Line 12

The resistivity characteristics of the collapse region cease to exist in the section from line 11 to line 14 and the contour of resistivity exhibits a nearly horizontal orientation. The lines 11–14 line profile bears resemblance to the line 12 line profile. The standard section consists of 12 lines. It is inferred that the low-resistance layer is mainly characterized by features of the fourth series, and a distinct zone of resistivity anomalies with a beaded pattern can be observed horizontally at depths ranging from 100 to 140 m. This anomaly zone is inferred to represent a mining roadway in the middle section of 310, which appears to be partially inundated with water, as depicted in Figure 17.

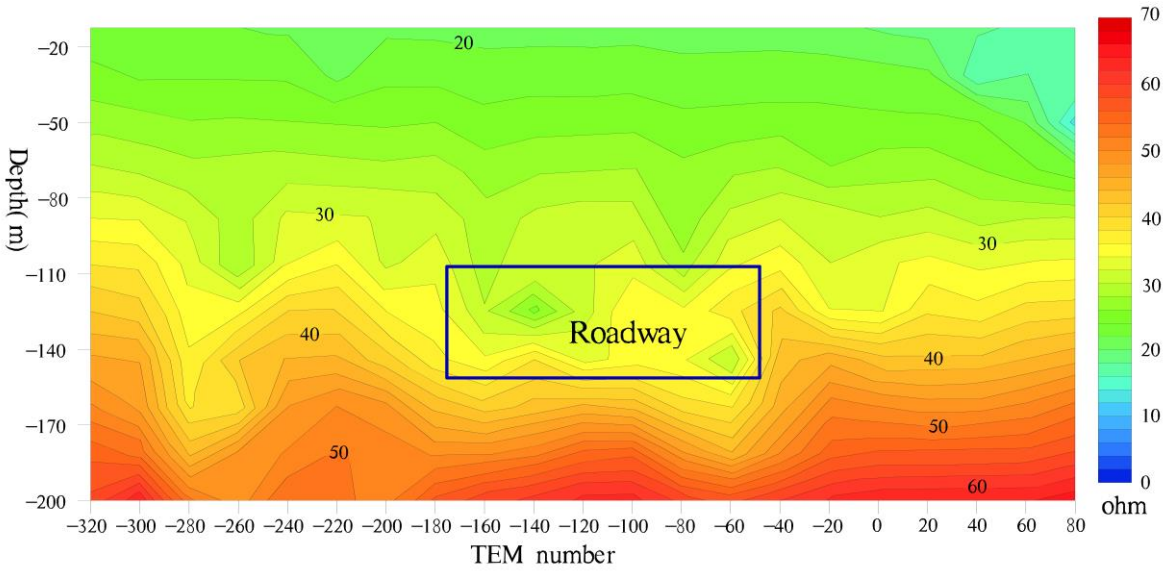

Figure 17. The diagram presents the inversion and interpretation of resistivity in survey line 12.

3.4. Result Analysis

The subsidence area was delineated by projecting the location onto the surface, using a division based on the 14 survey lines. The defined scope of this accident's subsidence area measured approximately 140 × 120 m. It exhibited a funnel-shaped morphology, with its center situated near −100 m to −60 m, along lines 3 to 4 of the survey line. The bottom

of the funnel represented the primary permeable point. Figure 18 illustrates the planar projection range of this subsidence area.

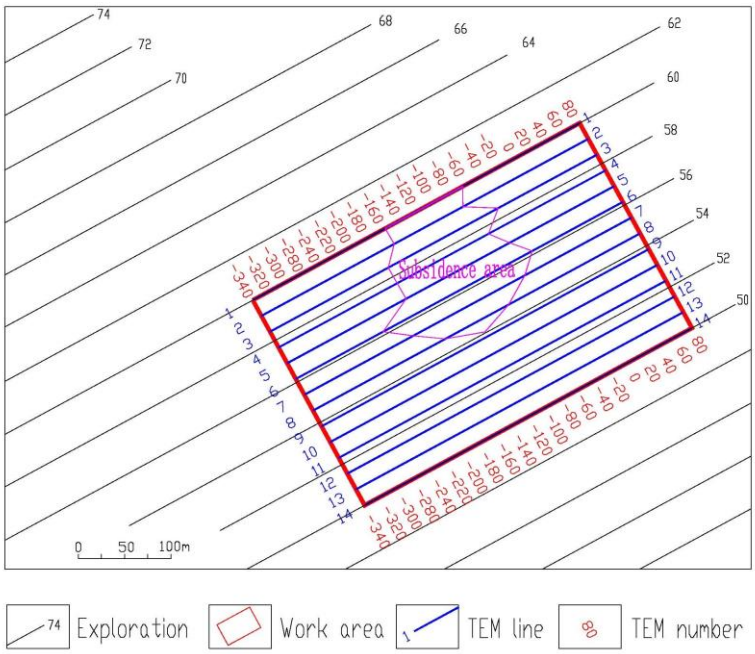

Figure 18. Subsidence area plane projection diagram.

In the middle section of work area 310, the roadway exhibits varying degrees of water accumulation from line 1 to line 12. Within the collapse area of lines 5 to 6 along the survey line, there is significant water filling in the middle section of 310, while noticeable reactions are observed only in lines 5, 9, and 10 along the survey line, in relation to the roadway within the middle section of 250. According to the resistivity characteristics, other survey line profiles indicate that there is no evidence of collapse or water filling in the middle section of 250 roadway.

3.5. Detection Result Verification

After blocking the underground roadway in the subsidence area, evident traces of water were discovered during the cleaning process in the central section spanning 310 m. The silting layer constituted approximately 10% to 25% of the roadway, with some sections displaying visible signs of water infiltration on top. However, within the middle segment, measuring 250 m, only partial indications of water presence were observed and the majority of the roadway exhibited no such evidence. Consequently, it can be inferred that the actual condition of water filling within the roadway aligns closely with the findings obtained through detection.

4. Advantages of the Ground-to-Air Transient Electromagnetic Method

The ground-to-air transient electromagnetic method involves placing the electrical source or loop source on the ground to induce excitation, while utilizing an airborne de-

vice to capture the corresponding electromagnetic response. The proposed method exhibits several advantages over conventional ground or aerial geophysical exploration techniques, including a highly responsive, well-conductive electrolyte; superior detection efficiency; minimal blind spots in detection; a significant depth of penetration; robust anti-interference capabilities; non-contact detection capability; cost-effectiveness; and enhanced safety [37–40].

In fact, during the investigation of this area, various methods were attempted in this study. However, only ground-to-air time domain electromagnetic detection was successful. During the high-density electrical detection data collection process, low current phenomena occur and geological data analysis indicates the presence of underground frozen soil shielding effects. Weak current phenomena still persist during controlled source audio magnetotelluric sounding launches. When excavated at the transmitting end, ice is found at a depth of about half a meter and there is a frozen layer between the transmitting and receiving ends, causing significant interference to the ground electrical method. High precision magnetic survey results reveal noticeable magnetic anomalies, which are interpreted as reactions from magnet ore bodies based on mining data.

In summary, the electrical detection results indicate the presence of underground permafrost, which gives rise to a high-resistance layer shield impeding surface electrical detection. The strong magnetic background poses challenges in distinguishing subsidence areas through high precision magnetic surveying. Moreover, the construction schemes employed solely rely on surface geophysical exploration work and are not directly applicable above subsidence areas, thus hindering the attainment of optimal outcomes.

The ground-to-air transient electromagnetic sounding method involves placing an electrical or loop source on the ground for excitation and utilizing a flight device to collect the corresponding electromagnetic response in the air. In comparison with conventional ground geophysical exploration methods, this approach offers the following several advantages: (1) Enhanced sensitivity to well-conductive electrolyte responses, enabling effective penetration of high-resistance underground regions, while exhibiting sensitive responses to low-resistance areas, thus making it highly suitable for detecting benign conductive media such as groundwater. (2) Wide applicability across diverse terrains including marshes, virgin forests, cliffs, deserts, and sea–land interaction zones; successful exploration has been achieved above water surfaces within subsidence areas during this project. (3) Robust anti-interference capabilities due to its working mode involving ground transmission and air reception; this allows receiving sensors to be positioned far away from ground noise sources, while maintaining strong adaptability within complex interference-prone regions near high voltage lines. And (4), high efficiency and cost-effectiveness owing to its ability to significantly reduce human labor and material expenses through efficient detection methodologies.

5. Conclusions

1. Through comparative analysis, the subsidence area, as a whole, exhibits a characteristic low resistance, with resistivity ranging between 5 and 15 Ω·m. The resistivity of the roadway displays significant variations, presenting a beaded resistivity anomaly. The water-filled roadway demonstrates a beaded low-resistivity anomaly, while the non-water-filled roadway exhibits a beaded high-resistivity anomaly.
2. The subsidence area, measuring approximately 140 × 120 m, is situated between survey line 1 and line 8 in a funnel-shaped manner. Due to the absence of survey line control on the northern side of survey line 1, the subsidence area remains open-ended, necessitating further exploration work.
3. The subsidence area is centered approximately −100 m to −60 m from line 3 to line 4 of the survey, with the main point of water permeation located at the bottom of the funnel.

4. The roadway in the middle section of mining area 310 exhibits a low impedance response from line 1 to line 12, which is influenced by subsidence and experiences varying degrees of water infiltration.
5. The middle section of 250 has evident low resistance reactions only at lines 5, 9, and 10 of the survey profiles, with partial water filling observed in the roadway. No significant low resistance is detected in other survey line profiles, indicating that most of the roadway in the middle section of 250 and below remains unaffected by collapse and is free from water accumulation.

Author Contributions: Conceptualization, Q.F. and C.L.; methodology, Q.F. and C.L.; validation, Z.S. and L.Z.; formal analysis, S.H.; investigation, D.L.; resources, T.L.; data curation, S.H.; writing—original draft preparation, Q.F., C.L. and S.H.; writing—review and editing, S.H.; funding acquisition, L.Z. All authors have read and agreed to the published version of the manuscript.

Funding: The study was funded by the Shandong Natural Science Foundation Youth Fund Project (ZR2021QD123) and the Jiangxi Geological Environment and Underground Space Engineering Research Center (grant No. JXDHJJ2022-013).

Data Availability Statement: Data is contained within the article.

Conflicts of Interest: The authors declare no conflict of interest.

References

1. Yi, D.; Jingrui, L. Research on Multi-parameter Interpretation Method of Advanced Exploration of Mine Transient Electromagnetic Method. In *Journal of Physics: Conference Series*; IOP Publishing: Bristol, UK, 2023; Volume 2660.
2. Zhu, Z.; Shan, Z.; Pang, Y.; Wang, W.; Chen, M.; Li, G.; Sun, H.; Revil, A.The transient electromagnetic (TEM) method reveals the role of tectonic faults in seawater intrusion at Zhoushan islands (Hangzhou Bay, China). *Eng. Geol.* **2024**, *330*, 107425.
3. Jubaedah, N.E.; Parnadi, W.W. On the application of Transient Electromagnetics (TEM) and DC-resistivity methods for groundwater level detection in the Cipatat karst area. In *IOP Conference Series: Earth and Environmental Science*; IOP Publishing: Bristol, UK, 2023; Volume 1288.
4. Chao, Q.F.; Gao, W.; Jian, Z.L. An Electromagnetic Scattering Reanalysis Method for Partial Geometry Modifications. *IET Microw. Antennas* **2023**, *17*, 701–709.
5. Ouyang, L.S. Progress in Ground Transient Electromagnetic Methods(TEM). *Earthq. Res. Sichuan* **2011**, *4*, 40–45.
6. Yang, G.; Chen, Y.J.; Jiang, Z.H. The Application of Small Loop TEM to Detecting Water in Goaf. *Chin. J. Eng. Geophys.* **2011**, *8*, 309–402.
7. Yang, Y.J.; He, Z.X.; Zhao, X.M. Research on The Defining All Time Apparent Resistivity of The TEM Method Excitated With Grounding Long Line Current Source. *Equip. Geophys. Prospect.* **2010**, *20*, 117–120.
8. Holladay, J.S.; Doll, W.E.; Beard, L.P.; Lee, J.L.; Gamey, T.J.; Bell, D.T. UXO Time Constant Estimation Form Helicopter Borne TEM Data. *J. Environ. Eng. Geophys.* **2006**, *11*, 43–52.
9. Guo, L.W. Study on The Method of Grounded-Wire TEM for WholeFied Exploration. Master's Thesis, Chengdu University of Technology, Chengdu, China, 2013.
10. Dai, Q.W.; Hou, Z.C.; Chai, X.C. Application of Transient Electromagnetic Method And EH-4 to Investigation of Mined-out Areas of Molybdenum Deposits. *Prog. Geophys.* **2013**, *28*, 1541–1546. (In Chinese)
11. Wang, P.; Zhang, W.; Li, J.; Deng, Z.; Wang, Y. Discussion on the Application of Integrated Aerogeophysical Method in Urban Site Selection and Construction. In *Journal of Physics: Conference Series*; IOP Publishing: Bristol, UK, 2023; Volume 2651.
12. Lei, D.; Hu, X.Y.; Zhang, S.F. Development Status Quo of Airborne Electromagnetic. *Contrib. Geol. Miner. Resour. Res.* **2006**, *21*, 40–53.
13. Fuxue, Y.; Yishu, S.; Yang, Z.; Jun, L. Design of High Transmission Frequency Circuit for Multiturn Small Loop Transient Electromagnetic Detection. In *Journal of Physics: Conference Series*; IOP Publishing: Bristol, UK, 2023; Volume 2651.
14. Zhang, C.D. Airborne Time Domain Electromagnetics system:Look Back and Ahead. *Chin. J. Eng. Geophys.* **2006**, *3*, 265–273.
15. Chen, J.J.; Liu, B.; Wang, P.L.; Yin, K.; Li, Y.; He, P. Application research of integrated geophysical exploration techniques to gypsum mine gob. *Prog. Geophys.* **2018**, *33*, 783–796. (In Chinese)
16. Feng, B.; Meng, X.H.; Zhang, B. Transmitting coil boundary effect for TEM large loop source and Elimination method. *Coal Geol. Explor.* **2010**, *38*, 61–66. (In Chinese)
17. Li, J.G.; Li, J.H. Application of transient electromagnetic method in coalmine gob area grouting effect detection. *Coal Geol. China* **2012**, *24*, 68–71. (In Chinese)
18. Yang, J.M.; Wei, Z.Z. The application of the methods of high density resistivity method and transient electromagnetic to detecting coal mining goaf and to inspect grouting effect. *Prog. Geophys.* **2014**, *29*, 362–369. (In Chinese)
19. Yu, J.C.; Li, Z.D. The high density resistivity method used for detecting foundation grouting. *Geol. Prospect.* **1998**, *34*, 48–51.

20. Nabighian, M.N. *Electromagnetic Methods in Applied Geophysics-Theory*; Society of Exploration: Tulsa, OK, USA, 1988; Volume 1, pp. 217–231.
21. Elliott, P. New Airborne Electromagnetic Method Provides Fast Deep-target Data Turnaround. *Lead. Edge* **1996**, *15*, 309–310.
22. Elliott, P. The Principles and Practice of FLAIRTEM. *Explor. Geophys.* **1998**, *29*, 58–60.
23. Mogi, T.; Tanaka, Y.; Kusunoki, K.I.; Morikawa, T.; Jomori, N. Development of Grounded Electrical Source Airborne Transient EM (GREATEM). *Explor. Geophys.* **1998**, *29*, 61–64.
24. Li, S.Y.; Lin, J.; Yang, C.H.; Tian, P.P.; Wang, Y.; Yu, S.B.; Ji, Y.J. Ground-Airborne electromagnelic signals de noising using a combined wavelet transiormalgorithm. *Chin. J. Geophys.* **2013**, *56*, 3145–3152, doi.10.6038/cig20130927.
25. Wang, Y.; Ji, Y.; Li, S.; Lin, J.; Zhou, F.; Yang, G. A Wavelet-based BaseLine Drift Correction Method for Grounded Electrical Source Airborne Transient Electromagnetic Signals. *Explor. Geophys.* **2013**, *44*, 229–237.
26. Ji, Y.J.; Wang, Y.; Xu, J.; Zhou, F.D.; Li, S.Y.; Zhao, Y.P.; Lin, J. Development and application of the grounded long wire source airborne electromagneliccxploration system based on an unmanned airship. *Chin. J. Crophys*. **2013**, *56*, 3640–3650, doi.10.6038cjg20131105. (In Chinese)
27. Cun, Z.; Qingsheng, B.; Penghua, H. A review of water rock interaction in underground coal mining: Problems and analysis. *Bull. Eng. Geol. Environ.* **2023**, *82*, 157.
28. Zhang, C.; Tu, S.; Zhao, Y. Compaction characteristics of the caving zone in a longwall goaf: A review. *Environ. Earth Sci.* **2019**, *78*, 27.
29. Zhang, C.; Chen, Y.; Ren, Z.; Wang, F. Compaction and seepage characteristics of broken coal and rock masses in coal mining: A review in laboratory tests. *Rock Mech. Bull.* **2024**, *3*, 100102.
30. Huang, D.R.; Lan, T.; Wu, Z.Y. Geological characteristics of Luotang gypsum deposit in Jiangxi province. *Resour. Surv. Environ.* **2011**, *32*, 137–142. (In Chinese)
31. Kong, F.N. Hankel transform filters for dipole antenna radiation in a conductive medium. *Geophys. Prospect.* **2010**, *55*, 83–89.
32. Yang, S.P.; Jiao, B.Q.; Sun, Z.J.; Zhang, X.J.;Xu, R.T.; Lu, X.P.; Pan, W.S.; Pu,X.Z. The Follow-up Methods for Regional Geochemical Anomalies in Forest-swamp Landscape Areas. *Geophys. Geochem. Explor.* **2008**, *32*, 480–487.
33. Han, G.; Liu, M.; Li, X.; Zhang, Q. Sources and geochemical behaviors of rare earth elements in suspended particulate matter in a wet-dry tropical river. *Environ. Res.* **2023**, *218*, 115044.
34. Ye, Y.X.; Deng, J.Z.; Li, M.; Yang, H.Y. Application status and vistas of electromagnetic methods to deep ore prospecting. *Prog. Geophys.* **2011**, *26*, 327–334. (In Chinese)
35. Kaufman, A.A.; Keller, G.V. *Frequency and Transient Soundings*; Elsevier Applied Science Publishers, Ltd.: London, UK, 2014.
36. Weir, G.J. Transient electromagnetic fields about an infinitesimally long grounded horizontal electric dipole on the surface of a uniform half-space. *Geophysics* **1980**, *61*, 41–56.
37. Liao, X.; Xu, Z.; Liu, W.; Tai, H.M.; Zhou, J.; Ma, X.; Fu, Z. Electromagnetic Detection System with Magnetic Dipole Source for Near-Surface Detection. *Sensors* **2023**, *23*, 9771.
38. Xue, G.Q.; Chen, W.Y.; Zhou, N.N.; Li, H. Short-off set TEM technique with a grounded wire source for deep sounding. *Chin. J. Geophys.* **2013**, *56*, 255–261. (In Chinese)
39. Xue, G.Q.; Pan, D.M.; Yu, J.C. Review the applications of geophysical methods for mapping coal-mine voids. *Prog. Geophys* .**2018**, *33*, 2187–2192. (In Chinese)
40. Hong, Z.Z.; Guang, H.W.; Xiao, D.P. Evaluation Method of Noise Electromagnetic Radiation Interference Effect. *IEEE Trans. Electromagn. Compat.* **2023**, *65*, 69–78.